Protein electron transfer: Dynamics and statistics

Dmitry V. Matyushov

Citation: The Journal of Chemical Physics **139**, 025102 (2013); doi: 10.1063/1.4812788

View online: http://dx.doi.org/10.1063/1.4812788

View Table of Contents: http://scitation.aip.org/content/aip/journal/jcp/139/2?ver=pdfcov

Published by the AIP Publishing

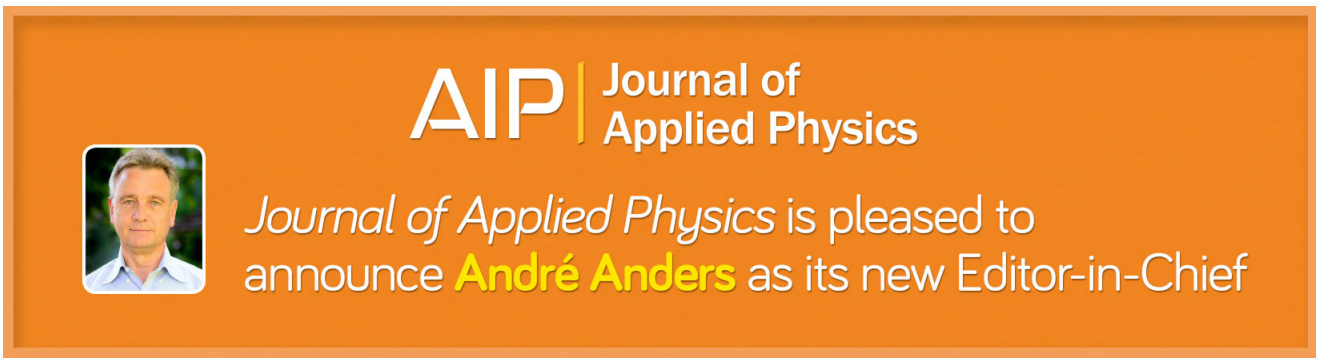

Protein electron transfer: Dynamics and statistics

Dmitry V. Matyushov[a)]
Center for Biological Physics, Arizona State University, PO Box 871504, Tempe, Arizona 85287-1504, USA

(Received 16 April 2013; accepted 18 June 2013; published online 11 July 2013)

Electron transfer between redox proteins participating in energy chains of biology is required to proceed with high energetic efficiency, minimizing losses of redox energy to heat. Within the standard models of electron transfer, this requirement, combined with the need for unidirectional (preferably activationless) transitions, is translated into the need to minimize the reorganization energy of electron transfer. This design program is, however, unrealistic for proteins whose active sites are typically positioned close to the polar and flexible protein-water interface to allow inter-protein electron tunneling. The high flexibility of the interfacial region makes both the hydration water and the surface protein layer act as highly polar solvents. The reorganization energy, as measured by fluctuations, is not minimized, but rather maximized in this region. Natural systems in fact utilize the broad breadth of interfacial electrostatic fluctuations, but in the ways not anticipated by the standard models based on equilibrium thermodynamics. The combination of the broad spectrum of static fluctuations with their dispersive dynamics offers the mechanism of dynamical freezing (ergodicity breaking) of subsets of nuclear modes on the time of reaction/residence of the electron at a redox cofactor. The separation of time-scales of nuclear modes coupled to electron transfer allows dynamical freezing. In particular, the separation between the relaxation time of electro-elastic fluctuations of the interface and the time of conformational transitions of the protein caused by changing redox state results in dynamical freezing of the latter for sufficiently fast electron transfer. The observable consequence of this dynamical freezing is significantly different reorganization energies describing the curvature at the bottom of electron-transfer free energy surfaces (large) and the distance between their minima (Stokes shift, small). The ratio of the two reorganization energies establishes the parameter by which the energetic efficiency of protein electron transfer is increased relative to the standard expectations, thus minimizing losses of energy to heat. Energetically efficient electron transfer occurs in a chain of conformationally quenched cofactors and is characterized by flattened free energy surfaces, reminiscent of the flat and rugged landscape at the stability basin of a folded protein. © *2013 AIP Publishing LLC*. [http://dx.doi.org/10.1063/1.4812788]

I. INTRODUCTION

This account addresses the effect of the statistics and dynamics of the donor and acceptor electronic states, localized inside hydrated proteins, on the kinetics of protein electron transfer. The main goal of the discussion is to highlight the differences, from the perspective of activating electronic transitions, between a dense polar solvent originally considered in the Marcus theory of electron transfer and a heterogeneous "solvent" composed of the protein and its hydration layer.

The development of the Marcus theory of electron transfer[1,2] was motivated by reactions of electron tunneling between solvated redox pairs, often represented by ions changing their redox state, as schematically shown by two redox states of a single solvated ion in Fig. 1(a). The original Marcus formulation has recognized the possibility of a heterogeneous (non-uniform) solvent surrounding the ion, distinguishing between the fluctuations of mostly bulk-like solvent outside the first hydration layer (outer-sphere reorganization) and the fluctuations of a tighter and less thermally agitated first hydration layer (inner-sphere reorganization). The collective motions of the inner shell are either frozen on the time-scale of electron transfer[3] or mostly eliminated by the layer's restructuring. Only ballistic, vibration-like motion of single molecules then contribute to a relatively small inner-sphere reorganization energy. Consequently, most of the fluctuations that the solvent provides to bring the donor and acceptor energy levels in resonance, as required for tunneling, are homogeneous (bulk-like). Translated into theoretical formalisms, approximations based on the properties of the homogeneous solvent provide a reasonable basis for quantitative theories.[4,5]

The thermal bath surrounding the protein redox site (iron of the protein heme shown as an example of protein electron transfer in Fig. 1(b)) is, on the contrary, fundamentally heterogeneous. Its two principal components are the protein matrix holding a redox cofactor (heme, chlorophyll, metal active site, etc.) and water of the hydration shell. The two regions are quite distinct in rigidity, dynamics, and the distribution of molecular charge. It is not only that the interface between a polymer and the water solvent is by necessity heterogeneous, the problem is complicated by the notoriously heterogeneous interface between the protein polymer and water.

[a)]Electronic mail: dmitrym@asu.edu

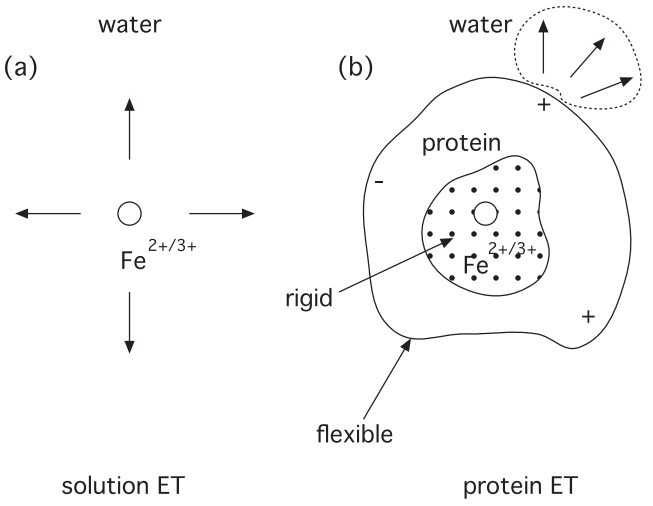

FIG. 1. Cartoon comparing the solvent bath of classical solution electron transfer (a) to heterogeneous protein-water thermal bath of protein electron transfer (b). The redox pair is represented by iron changing its oxidation state. It is a solvated ion in solution (a) and is a part of the heme cofactor in a redox protein (b). The protein part of the thermal bath is separated into a relatively rigid region of the heme and a flexible part of the protein-water interface. Ionized residues are predominantly located at the protein surface. They create electrostatically polarized and density compressed water domains at the interface. These domains combine into a heterogeneous and frustrated hydration shell of the protein with highly dispersive dynamics.

The energetic push for the protein to hold a stable folded structure requires ionized and polar residues to localize at its surface and to screen the protein hydrophobic core. Folding of a single chain of amino acids does not completely accommodate for this energetic preference and hydrophobic patches are still exposed to water (30%–50% of the protein surface[6]). The result is an electrostatically patchy surface of the protein,[7–9] producing, in turn, a patchwork of polarized and unpolarized domains of water facing it.[10,11] Water is known to orient its dipoles parallel to the dividing surface at hydrophobic patches[12,13] and flip its dipoles inward or outward depending on the surface charged group.[14–16] These heterogeneously polarized, heterogeneously compressed,[17–19] and potentially mutually frustrated interfacial water domains merge into an interfacial sub-ensemble involving several hundreds of water molecules, with its properties quite distinct from the bulk.[20,21] The bulk perspective does not apply just to the protein part of the thermal bath, but to the hydration shell as well.

Interfacial heterogeneity does not exhaust the list of new physical realities presented to protein electron transfer by the protein-water thermal bath. The once accepted picture of proteins as static hydrophobic media, covered by a layer of polar/ionized surface residues, has been mostly shaken by a large number of recent data pointing to a dynamic nature of proteins involving fluctuations of both the protein itself and the surrounding hydration shells.[22] The elastic network of the folded amino acid chain and, in addition, the hydration shell provide a large configurational space,[23,24] which a hydrated protein explores by a random walk through a large number of sub-states corresponding to nominally the same folded conformation.[25] Many of these motions produce elastic deformations altering either the shape of the protein or leading to protein domain motions (such as tumbling of α-helices).[8,26,27] Clearly, these elastic deformations project on motions of the charged surface residues and corresponding motions of water domains attached to them (Fig. 1(b)).[28] The result is a statistically broad spectrum of electrostatic fluctuations experienced by an active site. The dynamics of these fluctuations are also highly dispersive, covering many orders of magnitude in relaxation times.[29,30]

The question one has to address in relation to protein electron transfer is how all these new physical realities project on the energetics and dynamics of the donor-acceptor energy gap, which is the natural reaction coordinate for studying radiationless transitions.[31–37] That some of the traditional concepts need revision is already clear from many reports of the Stokes shift dynamics of chromophores placed either at the protein-water interface or within the protein. Time-resolved Stokes shift spectroscopy of chromophores attached to proteins universally reports slow dynamics not recorded by the same chromophores in solution.[38–42] There obviously are some nuclear modes, interacting with the chromophore's dipole moment, which are either absent in the bulk solvent or alter their dynamics in the vicinity of the hydrated protein.

The picture offered below incorporates two distinctive properties of the protein-water thermal bath into the description of protein electron transfer: (i) a wide breadth of electrostatic fluctuations created by the flexible protein-water interface and (ii) dispersive dynamics (the existence of many relaxation times) associated with these nuclear fluctuations. The first feature is responsible for shallow, low-curvature free energy surfaces along the electron transfer reaction coordinate.[43] This observation implies a large magnitude of the nuclear reorganization (free) energy λ^{var} associated with the free energy curvature. The second feature addresses the separation between the minima of the free energy surfaces. Their separation, $\Delta X = 2\lambda^{St}$ in Fig. 2, is related to the Stokes shift in optical spectroscopy (the subscript "St" stands for "Stokes"). This reorganization energy can be modified by dynamical freezing of some subsets of the nuclear modes affecting the donor-acceptor energy gap.

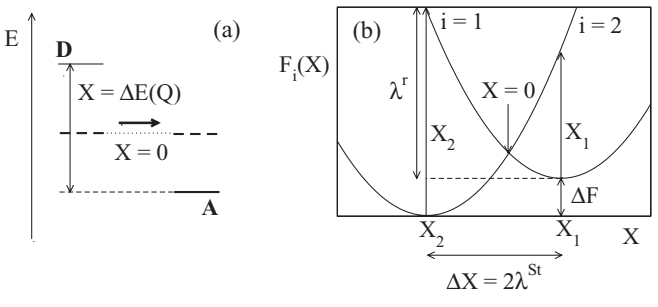

FIG. 2. (a) The energy diagram showing the energy gap between the donor and acceptor as the electron-transfer reaction coordinate, $X = \Delta E(Q)$. The condition of resonance, $X = 0$, defines the transition state in which electron tunnels from the donor to the acceptor. (b) The diagram of free energy surfaces $F_i(X)$ vs. the reaction coordinate X. The minima of the parabolas are located at X_i, $i = 1, 2$ and the parabolas cross at $X = 0$. Two out of three alternative definitions of the reorganization energy discussed in the text are specified in the plot; ΔF is the reaction free energy.

The wide breadth of electrostatic fluctuations associated with elastic motions of the protein-water interface requires, by its collective nature, relatively long relaxation times. Simulations of hydrated proteins consistently report sub-nanosecond to nanosecond relaxation times associated with these modes.[30,44,45] These time-scales have also been reported experimentally by measurements of the Stokes-shift dynamics.[40,46–50] These, and possibly even longer,[28] electrostatic relaxation times create the possibility for breaking the ergodicity of the system and making some parts of the protein-water phase space inaccessible on the time-scale of the reaction or on the time-scale of electron residence on a cofactor in a redox chain.[51,52] The resulting dynamical arrest of corresponding nuclear modes, an almost trivial and common phenomenon in glass science,[53] does not allow full statistical averages to develop on the limited time-scale of the reaction.[54]

In terms of protein electron transfer occurring on the nanosecond time-scale, this picture implies that the distance, along the reaction coordinate, between the minima of the free energy surfaces cannot be characterized by the same nuclear reorganization parameter as the curvature at the free energy's bottom.[52] If $\lambda^{\rm St}$ is used for the former (Fig. 2) and $\lambda^{\rm var}$ is used for the latter, the distinction between the two reorganization energies can be characterized by the parameter

$$\chi_G = \lambda^{\rm var}/\lambda^{\rm St}. \tag{1}$$

When the same Gaussian statistics of the energy gap is applied to both redox states, one gets $\chi_G = 1$.[55] The parameter based on two distinct reorganization energies therefore quantifies the globally non-Gaussian statistics of the donor-acceptor energy gap. We assign the label "globally non-Gaussian" to the inability of fitting the distributions of the energy gap in both electronic states to Gaussians with mutually consistent sets of parameters (see below). The main observation from a number of numerical simulations and some experiments is that the following inequality holds for protein electron transfer:

$$\chi_G \geq 1. \tag{2}$$

The actual magnitudes of χ_G can significantly exceed unity.[52]

The consequences of this perspective for the performance of biology's energy chains are quite dramatic, as we discuss below, since the energy released in the form of heat in activationless electron transfer can be reduced by a factor of χ_G. The ability of proteins to increase χ_G is therefore directly related to their performance as energetically efficient enzymatic machines. This picture explains the remarkable energetic efficiency of electron transport chains in biology, often operating in narrow windows of redox potentials.[56] It also offers possible routes to implement this design strategy in artificial photosynthesis.

II. MECHANISTIC FEATURES OF PROTEIN ELECTRON TRANSFER

The modern formulation of the electron transfer theory utilizes the notion, going back to Lax,[31] that the instantaneous energy gap between the electronic energy levels of the acceptor and the donor makes the natural choice for the reaction coordinate of radiationless transitions (Fig. 2(a)).[32–36] This reaction coordinate is a "collective variable," influenced by many molecules interacting with the two electronic states. If the corresponding manifold of the nuclear coordinates is denoted as Q, then each magnitude of the donor-acceptor gap $\Delta E(Q)$ should satisfy the condition $X = \Delta E(Q)$.

The probability to find a particular energy gap is obtained by projecting the canonical statistical ensemble on the free energy surfaces $F_i(X)$, where we use $i = 1$ for the initial state and $i = 2$ for the final state. This projection is accomplished mathematically by tracing the canonical distribution, while separating out a subset of coordinates satisfying the condition $X = \Delta E(Q)$ through Dirac's delta-function[33,36]

$$e^{-\beta F_i(X)} \propto \langle \delta\left(X - \Delta E(Q)\right)\rangle_i. \tag{3}$$

Here, $\langle \ldots \rangle_i$ refers to an ensemble average when the system is in equilibrium with the donor-acceptor complex in its electronic state $i = 1, 2$; $\beta = 1/(k_{\rm B}T)$ is the inverse temperature.

Given that many atomic and molecular coordinates contribute to Q, and assuming a linear coupling between the donor-acceptor complex and the thermal bath,[55] one can expect that, according to the central limit theorem, the distribution $P_i(X)$ of energy gaps should be Gaussian

$$P_i(X) \propto e^{-\beta F_i(X)} \propto \exp\left[-\frac{(X - X_i)^2}{2\langle(\delta X)^2\rangle_i}\right]. \tag{4}$$

This is the central assumption of the Marcus theory, which can be cast in the form of two parabolic free energy surfaces

$$\begin{aligned} F_1(X) &= \frac{(X - X_1)^2}{4\lambda^{\rm var}}, \\ F_2(X) &= \frac{(X - X_2)^2}{4\lambda^{\rm var}} + \Delta F. \end{aligned} \tag{5}$$

In this equation, X_i is the average energy gap, which specifies the location of the minimum of each parabola. At the same time, X_i is the energy of the vertical charge-transfer transition between the ground and optically excited states (Fig. 2).

The reorganization energy

$$\lambda^{\rm var} = \beta\langle(\delta X)^2\rangle/2 \tag{6}$$

in the denominator of the parabolas specifies the variance of the Gaussian distribution in Eq. (4), as is reflected by the subscript "var." It is accessible from inhomogeneous broadening of a single vibronic transition in optical spectra.[57] Note that we have dropped the dependence on the state in the ensemble average and in the corresponding reorganization energy in Eq. (6). The difference between $\lambda^{\rm var}$ values is two electronic states is not a major effect for our present consideration, although it becomes important for systems involving significant changes in the electronic polarizability upon electronic transition.[55,58]

The distance between the minima of the parabolas specifies another spectroscopically measurable quantity, the Stokes shift.[57] We specify the corresponding reorganization energy as the half of it,

$$\lambda^{\rm St} = \Delta X/2 = |X_1 - X_2|/2. \tag{7}$$

The two reorganization energies, $\lambda^{\rm var}$ and $\lambda^{\rm St}$, which have been specified so far to reflect the information available from spectroscopic data, are distinct from the reorganization energy defined in the traditional formulation of the Marcus theory focused on electron-transfer (radiationless) reactions.[1] Specifically, the reorganization energy of "horizontal,"[59] in contrast to "vertical" Franck-Condon, transition is defined as the free energy (reversible work) required to drive the system, remaining in a given electronic state, from its initial equilibrium nuclear configuration to the final nuclear configuration, i.e., the distance $|\Delta X|$ along the reaction coordinate. This reorganization energy, which we denote λ^r, is given by the relation

$$\lambda^r = \frac{(\lambda^{\rm St})^2}{\lambda^{\rm var}} = \frac{\lambda^{\rm St}}{\chi_G}, \tag{8}$$

where χ_G is specified by Eq. (1).

The reorganization energy $\lambda^r = -\Delta F$ has an important property to measure the free energy released to the surrounding medium in an activationless ($\Delta F^\dagger = 0$) reaction, where $\Delta F^\dagger$ is the activation free energy.

The complexity of several alternative definitions of the reorganization energy does not appear in the standard formulation of the Marcus theory, in which all reorganization energies defined above are equal.[57] Different definitions provide alternative routes to the same theory parameter. This is easy to show by applying the linear relation between the two free energy surfaces[35] to Eq. (5),

$$F_2(X) = F_1(X) + X. \tag{9}$$

This relation is a property of the canonical ensemble.[60] From this additional requirement, one gets one single reorganization energy λ required to describe both optical and thermally activated transitions,

$$\lambda^{\rm var} = \lambda^{\rm St} = \lambda^r = \lambda. \tag{10}$$

In addition to this relation, one gets $\Delta F = \bar{X} = (X_1 + X_2)/2$, thus reducing the model to two independent parameters.

Several alternative definitions of the reorganization energy are introduced here because Eq. (10) breaks down for protein electron transfer, requiring two separate reorganization energies to determine the electron-transfer energetics, $\lambda^{\rm St}$ and $\lambda^{\rm var}$; the reorganization energy λ^r is defined by them via Eq. (8).

Electronic transitions occur by tunneling when zero energy gap between the donor and acceptor, $X = 0$, is reached (Fig. 2). The activation barrier for $1 \rightarrow 2$ reaction follows from the probability of reaching the $X = 0$ point on the reaction free energy surface. From Eq. (4) one gets

$$\Delta F^\dagger = \frac{(X_1)^2}{4\lambda^{\rm var}} = \frac{(\lambda^{\rm St} + \Delta F)^2}{4\lambda^{\rm var}} \rightarrow \frac{(\lambda + \Delta F)^2}{4\lambda}, \tag{11}$$

where the equality between the reorganization energies [Eq. (10)] is used in the last transformation.

One has to stress that the sum of $\lambda^{\rm St}$ and ΔF in Eq. (11), each of which is a free energy, makes the average (vertical) transition energy. This constraint implies that the entropy parts of $\lambda^{\rm St}$ and ΔF cancel out in the sum. This requirement is in fact stipulated by the Franck-Condon principle demanding stationary nuclei during an optical transition. Since the nuclei do not move on the transition timescale, there is no entropy change associated with a vertical transition.

III. DYNAMICS OF THE ENERGY GAP AND NONERGODIC KINETICS

Electron transfer is promoted by nuclear fluctuations affecting the donor-acceptor energy gap. The spectrum of these fluctuations is therefore of main interest for the theory development. In spectroscopy, temporal changes of the transition energy are commonly associated with the Stokes-shift dynamics.[61–63] The dynamics of small fluctuations around equilibrium are identical to the dynamics in response to a small perturbation,[64] and so we will use the term "Stokes-shift dynamics" for the dynamics of near-equilibrium fluctuations of X.

The relaxation of a small deviation from equilibrium $\delta X_i(t) = X(t) - X_i$ can be followed by monitoring the time self-correlation function

$$S_i(t) = [\langle(\delta X_i(0))^2\rangle]^{-1}\langle\delta X_i(t)\delta X_i(0)\rangle. \tag{12}$$

Its Fourier transform leads to the loss function,[64] $\chi''(\omega) = \beta\omega S(\omega)/2$. Here, as above, we have dropped the index "i" from both $S_i(t)$ and $\chi_i''(\omega)$. The loss function quantifies the dissipation of energy to the surrounding thermal bath upon changing the redox state or charge distribution of the donor-acceptor complex. The peaks of $\chi''(\omega)$ tell about the characteristic relaxation times of the nuclear modes coupled to the donor-acceptor energy gap and their heights quantify relative weights of these modes in the overall solvent reorganization energy.

Molecular charge-transfer complexes, which have been extensively studied over the last several decades,[63] are characterized by two types of nuclear modes affecting electronic transitions. The skeletal vibrations of the complex itself are typically in the high-frequency region, exceeding $k_{\rm B}T$ in energy.[65] The second, slower mode is assigned to the solvent. It has two characteristic time-scales: ballistic motions, on the time-scales of $<$100 fs,[66] and collective orientational motions of the solvent multipoles, on the picosecond time-scale.[61,67]

The splitting of the fluctuation spectrum into the high-frequency and low-frequency parts is accommodated in the Marcus theory by separating the reorganization energy into the high-frequency, intramolecular, and low-frequency solvent components. The intramolecular contribution is small for rigid binuclear charge-transfer complexes,[68] but might be significant for organic compounds.[65] It is typically small for cofactors participating in protein electron transfer.[69] It has been argued that the combination of a rigid structure of the cofactor with delocalization of the transferred electron over a number of its atoms helps to reduce intramolecular reorganization[70] and, by that, the energy penalty of elastic deformation caused by transferring the electron.

Reasons for the overall small intramolecular reorganization energy are not well understood. It is clear that the heme cofactor presents a rigid subunit with a low intramolecular

reorganization energy.[71] Why the deformation caused by altering the redox state either does not propagate further inside the protein or, when propagating,[72] does not affect the reorganization energy has not been fully addressed. A part of the reason might be assigned to a typically weak coupling of the heme to the rest of the protein; many redox proteins hold the heme in the folded position by non-bonded interactions only, while a flexible linker is present in others.[73] Irrespective of the reasons, there are indications of a small magnitude of the internal reorganization energy in proteins transferring electrons[69] and general conservation of their structure in different redox states.[74] We, therefore, focus here on the solvent component of nuclear reorganization, by which we mean reorganization of the strongly coupled protein-water solvent. In anticipation of the results discussed below, the protein-water thermal bath is mechanistically viewed as a combination of a rigid core in the nearest vicinity of the redox center and a flexible interfacial region surrounding it. It is the latter part that is responsible for a broad spectrum of electrostatic fluctuations affecting the active site (Fig. 1(b)).

The dynamics of the protein-water solvent are significantly more complex than the dynamics of a typical polar molecular liquid. Two distinctions are particularly noteworthy. First, the spectrum of relaxation times is broad, i.e., many characteristic relaxation times can be identified. Second, there is a significant excess of slow relaxation times, extending down to conformational transitions at the millisecond timescale for single-domain proteins, or even longer time-scales for multidomain proteins.[75] This new physical reality requires new theoretical approaches to describe protein electron transfer, which we discuss next.

The reorganization energy is defined in the Marcus theory as canonical, equilibrium free energy. This definition carries with it the assumption that all degrees of freedom contributing to λ are significantly faster than the observation time $\tau_{\rm obs} = k^{-1}$, which is the inverse of the reaction rate k for electron-transfer reactions. This condition is typically satisfied for not too fast reactions in polar molecular solvents, but often becomes compromised for the protein-water solvent.[52] The protein-water thermal bath becomes nonergodic when the reaction rate exceeds one of the characteristic relaxation frequencies (peaks) in $\chi''(\omega)$. There is of course nothing specific to protein in this phenomenon, which is also realized for redox couples in solution.[49,51,76–78] Specific to proteins is a substantial weight of low-frequency modes in the overall reorganization energy, which makes this effect significant numerically.

To illustrate the origins of nonergodicity, Fig. 3 shows the typical Stokes-shift loss function calculated from atomistic simulations (~100–150 ns Molecular Dynamics (MD) trajectories) of two hydrated proteins, cytochrome *c* (cytC),[30] and green fluorescent protein (GFP).[45] In the former case, the energy gap coordinate corresponds to changing the oxidation state of the iron of the heme, in the latter case the energy gap is between the ground and excited singlets of GFP's chromophore. The characteristic feature of several such functions reported so far[30,45,79] is the existence of two peaks, with a possibility that even slower relaxation times are still not resolved on the length of the simulation trajectory.

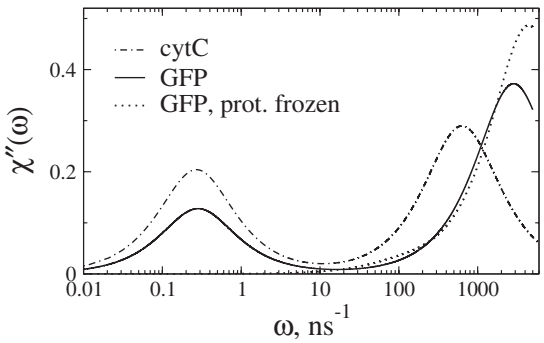

FIG. 3. Stokes-shift loss function $\chi''(\omega)/\chi'(0)$ for cytochrome *c* (cytC)[30] and green fluorescent proteins (GFP)[45] obtained from MD simulations. The dotted line indicates simulations in which the motions of both the protein and the GFP chromophore were frozen during the simulation run. The results for GFP report the loss function calculated in the excited S1 singlet of the chromophore.

The faster relaxation component is characteristic of the water shell, slowed down compared to the bulk by the presence of a large solute,[80] and intramolecular localized vibrations of the protein. The slower component in $\chi''(\omega)$ arises from the coupled elastic motions of the protein and its hydration shells. This attribution is clearly demonstrated by the disappearance of the slow peak when the protein is frozen,[45,81] as is shown by the dotted line in Fig. 3. In addition, when the overall spectral density is split into the water and protein components, their corresponding low-frequency peaks point to nearly equal relaxation times.[45,79] This observation indicates that the protein and water motions contributing to the low-frequency relaxation are strongly coupled. These nuclear modes are specific to the elastically soft hydrated protein. They are not observed for molecular charge-transfer complexes dissolved in polar liquids, for which the Marcus theory has been extensively tested.[5,82]

The existence of nanosecond relaxation modes, and perhaps still unresolved slower relaxation components,[83] carries a profound consequence for protein electron transfer occurring on nanosecond and sub-nanosecond time-scales. The variance reorganization energy in Eq. (6) can be calculated by integrating the entire loss spectrum of the Stokes shift dynamics,

$$\lambda^{\rm var} \propto \int_0^\infty \chi''(\omega)(d\omega/\omega). \tag{13}$$

Because of the ω^{-1} scaling, the low-frequency components of the loss spectrum are most important.

Once again, Eq. (13) applies when $k \ll \tau_j^{-1}$, where τ_j are the characteristic relaxation times responsible for the peaks in $\chi''(\omega)$ (Fig. 3). If this condition is violated, the low-frequency motions do not participate in fluctuations of the donor-acceptor energy gap and the above equation for the thermodynamic reorganization energy needs to be replaced with a nonergodic (non-canonical) reorganization energy[51,54,84] depending on the rate constant k,

$$\lambda^{\rm var}(k) \propto \int_k^\infty \chi''(\omega)(d\omega/\omega). \tag{14}$$

If the Stokes shift relaxation function $S(t)$ [Eq. (12)] is approximated by a multi-exponential decay, Eq. (14) leads to a simple formula for the reorganization energy,

$$\lambda^{\rm var}(k) = f(k)\lambda^{\rm var}. \tag{15}$$

Here, $\lambda^{\rm var}$ is the thermodynamic (canonical) reorganization energy in Eqs. (6) and (13) and the nonergodicity coefficient is

$$f(k) = (2/\pi)\sum_j A_j \,{\rm arccot}\left(k\tau_j\right), \quad \sum_j A_j = 1, \tag{16}$$

where A_i are the relative weights of the relaxation components in $\chi''(\omega)$.

The nuclear motions affect not only the reorganization energy, but also the reaction free energy ΔF. Therefore, the need for a nonergodic correction does not stop at $\lambda(k)$. Empirically, one might replace ΔF with $\Delta F(k)$, if the vertical separation between the free energy minima can be measured on the same time-scale as the reaction. However, the reaction free energy becomes ill-defined and the advantage of an independent experimental input, which had prompted the splitting of the average vertical energy gap X_i into ΔF and λ,[1] is mostly lost. One can therefore switch back to the average energy gap, which then becomes a function of the reaction rate as well,[58]

$$X_i(k) = X_{\rm np} + f(k)X_i^C. \tag{17}$$

In this equation, the average energy gap is separated into the components $X_{\rm np}$ and X_i^C. The former is the sum of the gas-phase energy gap and dispersion and induction interactions between the transferred electron and (fast) electronic degrees of freedom of the protein-water solvent. The latter, X_i^C, is the Coulomb interaction of the transferred electron with partial atomic charges moved by (slow) nuclear modes. The Coulomb component is affected by the nonergodic cutoff of the loss spectrum and, therefore, requires the nonergodicity coefficient $f(k)$.

IV. NONERGODICITY AND GLOBALLY NON-GAUSSIAN STATISTICS

The nonergodic effects discussed here originate from the difficulty to separate the time-scales of nuclear relaxation from the time-scale of the reaction. The discussion so far has followed the logic of the Marcus picture assuming that the polarization fluctuations of the bath occur near its equilibrium configuration, with both the initial and final equilibrium configurations equally accessible. We now turn our attention to a view of the electron-transfer reaction in terms of two reaction coordinates,[85–88] the already discussed polarization of the protein-water interface and, in addition, a reaction coordinate representing conformational transitions of the protein caused by changing redox state.

In contrast to relatively fast fluctuations of the interfacial polarization, ranging from ps to ns in relaxation times, conformational transitions require passing high activation barriers and, therefore, can be slow, spanning the μs to ms time-window.[22,89] Many electron-transfer steps within biological electron transport chains are faster,[56] and that again creates conditions for dynamical freezing of the modes slow compared to the reaction rate.

The loss of ergodicity in the phase space of protein conformational transitions projects itself on the separation between $\lambda^{\rm St}$ and $\lambda^{\rm var}$ reorganization energies. While access to the protein high-frequency vibrations and lower-frequency dissipative elastic motions around only one of the conformational equilibria is required for producing $\lambda^{\rm var}$, both equilibrium states are required to determine $\lambda^{\rm St}$. Inaccessibility of one of the conformational states limits $\lambda^{\rm St}$ to the manifold of polarization modes only, while allowing both the polarization and protein vibration/elastic modes to affect $\lambda^{\rm var}$.

This situation is schematically illustrated in Fig. 4. We show two coordinates in the plot, one representing the polarization fluctuations of the coupled protein-water system, as quantified by the loss function $\chi''(\omega)$, and the other representing conformational changes in the protein caused by changing the redox state. The total Stokes shift reorganization energy requires both fast changes of the interfacial polarization and a conformational transition of the protein. If the residence time of the electron on a given cofactor is long and the system has sufficient time for a slow conformational change, one should reach the equilibrium limit of Gaussian fluctuations within the canonical ensemble, characterized by $\lambda^{\rm St} = \lambda^{\rm var}$ [Eq. (10))] and $\chi_G = 1$ [Eq. (2)]. This situation is marked in Fig. 4 by a diagonal (dashed line) transition path connecting the two fully equilibrated configurations.

In the other limiting case of the residence time short compared to the time of conformational transition, the reaction ends at a local minimum along the polarization P-axis in Fig. 4. Electro-elastic fluctuations of the interface allow a number of trajectories to reach the local minimum along the

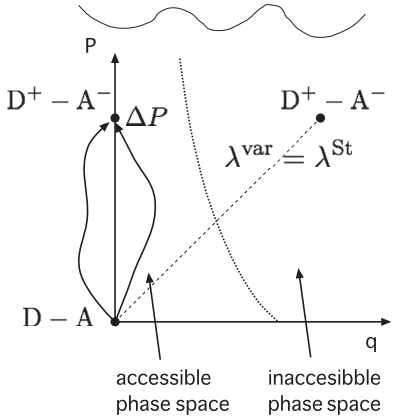

FIG. 4. Cartoon illustrating ergodicity breaking of electron transfer involving two collective coordinates: (i) fast (∼ns–ps) coordinate P representing polarization of the protein-water interface and (ii) slow (ms–μs) coordinate q representing conformational transition caused by changing redox state. The dashed diagonal line represents the pathway between two equilibrium states along which the standard prescriptions of Gaussian statistics with $\chi_G = 1$ apply. For a reaction faster than the time-scale of conformational transition along the q-coordinate, only the local minimum along the fast reaction coordinate P is reached. Since the trajectories are spread by fluctuations around the equilibrium conformation of the initial state, one gets $\chi_G > 1$. Many local minima, shown by the wiggled line on the top, might exist along the q-coordinate and, therefore, a number of outcomes approaching $\chi_G = 1$ are possible when the reaction time becomes longer, approaching the time of establishing the conformational equilibrium.

P-coordinate, which is indicated by several alternative transition paths in Fig. 4. Formally, this situation can be described by requiring the energy gap coordinate to be a linear function of two Gaussian variables, P and q: $X = aP + bq$. The statistical average in Eq. (3) is then taken over the Gaussian variable P, which is allowed to have two equilibrium values corresponding to two local minima along the P-axis, and variable q, which is allowed only one equilibrium value. If κ_P and κ_q are two force constants for harmonic displacements along the P and q coordinates, respectively, one gets $\lambda^{\rm var} = a^2/(2\kappa_P) + b^2/(2\kappa_q)$. On the other hand, if ΔP is the distance between the two minima along the P-axis, one gets $\lambda^{\rm St} = a\Delta P/2$. As discussed above, one has to violate the linear relation in Eq. (9) between the two free energy surfaces to allow $\chi_G \neq 1$. If that happens, one gets $F_2(X) - F_1(X) = X/\chi_G + {\rm Const}$.

If the standard relations of linear response are satisfied along the P-axis, one has $a\Delta P = a^2/\kappa_P$ and, therefore, $\lambda_P^{\rm var} = \lambda_P^{\rm St} = \lambda^{\rm St}$. At the same time, because $b^2/(2\kappa_q)$ term is a part of $\lambda^{\rm var}$, one gets $\lambda^{\rm var} > \lambda^{\rm St}$ and $\chi_G > 1$. All that is required to arrive at this result is to use a restricted ensemble[90] (dynamically restricted ensemble for kinetic applications[51]) defined on a portion of the phase space, instead of the canonical ensemble defined on the entire phase space of the system. In other words, nonergodic statistical average is not defined by the Hamiltonian alone, but involves an additional information on the phase space dynamically allowed to the system, effectively an entropic term. Thus X is an energy function specifying the change of the coupling to the bath upon electronic transition, but, because of nonergodicity, it is not the same function as the one involved in the statistical average. The result is a breakdown of the linear relation in Eq. (9) specific to the canonical ensemble.

An alternative way to think about separate trajectories reaching the local minimum on the P-axis (Fig. 4) is a random walk of the protein through nearly iso-energetic sub-states at the bottom of the stability basin.[91] Since each sub-state has a slightly different conformation, it will produce a different coupling of the quantum energy level of the localized electron to the polarization of the protein-water solvent. As a result, each sub-state will produce a separate reaction pathway. The statistics of just a few sub-states will lead to a superposition of parabolas in $F_i(X)$, each weighted with its Boltzmann factor.[92] Alternatively, when there is a large number of nearly iso-energetic sub-states, such as in a fragile glass-former,[53] their couplings to the reaction coordinate will be spread according to a Gaussian distribution. One then immediately arrives at Eq. (5). If, additionally, the distribution of sub-states is an "intrinsic property" of the protein, not affected by electronic transition, the result is $\lambda^{\rm var} > \lambda^{\rm St}$ and $\chi_G > 1$. Whether a new conformational state that can potentially alter the distribution of sub-states is not kinetically reached or is too high in free energy thermodynamically is irrelevant here. The main point is that the corresponding part of the phase space is inaccessible, and that simple fact requires two separate reorganization energies to describe the reaction. Further, a non-Gaussian protein landscape projects on non-parabolic free energy surfaces. For instance, a square-well landscape produces non-parabolic $F_i(X)$ flattened at the bottom.[93]

Simulations report quite significant values of χ_G when the trajectories in two redox states are started from the same protein conformation and their length is insufficient to sample alternative conformations. The laboratory situation might of course be everything in between of two limiting cases: the transition along the P-axis or along the equilibrium path shown by the dashed line in Fig. 4. The flat bottom of the basin of stability of a typical folded protein[89] suggests that there might be many local conformational minima (shown by the wiggled line in Fig. 4) on the way of the overall conformational transition connecting the local minimum on the P-axis to the global equilibrium minimum in the $P-q$ plane. What this perspective practically implies is that a number of possible outcomes for the magnitude of χ_G are possible, depending on the residence time of the electron on a cofactor within the electron transfer chain. Natural electron transfer chains have potentially taken advantage of this possibility, as we discuss below.

V. ELECTRO-ELASTIC FLUCTUATIONS OF THE PROTEIN-WATER INTERFACE

The nonergodic separation between the Stokes shift $\lambda^{\rm St}$ and variance $\lambda^{\rm var}$ reorganization energies discussed above is only efficient if $\chi_G \gg 1$, i.e., when $\lambda^{\rm var}$ is large. A large amplitude of electrostatic noise produced by elastically flexible protein-water interface is therefore quite essential for this new mechanistic picture of protein electron transfer. These electrostatic fluctuations are caused by coupled protein-water elastic deformations occurring on the sub-nanosecond time-scale (low-frequency peak in $\chi''(\omega)$ in Fig. 3). They move protein surface charges and, adiabatically, domains of surface water, polarized by the protein and attached to it by surface hydrogen bonds (Fig. 1(b)).

In an attempt to understand the origin of intense electrostatic fluctuations, and qualitatively describe them, a natural approach is to look at the contributions to $\lambda^{\rm var}$ from the protein and hydration shell separately. This approach is straightforward for the Stokes shift, which can be separated into the protein (p) and water (w) components

$$\lambda^{\rm St} = \lambda_p^{\rm St} + \lambda_w^{\rm St}. \tag{18}$$

In contrast, $\lambda^{\rm var}$ involves a cross-term, $\lambda_{pw}^{\rm var}$,

$$\lambda^{\rm var} = \lambda_p^{\rm var} + \lambda_w^{\rm var} + \lambda_{pw}^{\rm var}. \tag{19}$$

A direct application of the linear-response approximation,[64] equivalent to the Gaussian statistics in the fully equilibrated canonical ensemble, suggests the following connection between the Stokes-shift and variance components:

$$\lambda_{p,w}^{\rm St} = \lambda_{p,w}^{\rm var} + \tfrac{1}{2}\lambda_{pw}^{\rm var}. \tag{20}$$

Equation (20) thus indicates that one cannot apply linear response to a single component only and, instead, cross-correlations have to be involved.[94,95] This general result is not limited to electron-transfer reorganization and becomes important in other areas as well, e.g., for the dielectric response of protein solutions.[96,97]

The relative contributions of the protein and water to λ^{St}, and its total magnitude, are strongly affected by the proximity of the redox site to the interface.[44] However, water and protein contributions to λ^{St} are typically of similar magnitudes. For instance, $\lambda^{St} = 1.07$ eV for the half-reaction of changing the redox state of protein plastocyanin is split into 0.60 eV from protein and 0.47 eV from water.[11] Similarly, λ^{St} of primary charge separation in bacterial photosynthesis, calculated from long simulations trajectories (i.e., referring to $k \to 0$), is about 0.76 eV, and is split into 0.41 eV from protein and 0.35 eV from water.[98] The reorganization energy referring to the fast reaction rate of photosynthetic charge separation, $\tau_{obs} \simeq 0.3\ ps^{-1}$, is reduced to 0.36 eV according to the nonergodic cutoff described by Eqs. (14) and (17).

Overall, neither the proposal that protein is a hydrophobic environment producing little reorganization energy nor the idea that water is sufficiently screened from affecting electron transfer are supported by simulations. A typical protein redox center is affected by both components of the protein-water solvent, and the protein surface contains a sufficient number of movable polar/charged groups to act as a polar solvent. The latter point also implies that care is required with the idea that a significant reduction of the reorganization energy may be achieved in protein complexes, when bulk water (but hardly the first hydration layer) is removed from the contact area. The fact that many redox proteins form highly transient complexes, with many nearly isoenergetic configurations[99,100] suggests that no significant enhancement of the rate is achieved in a particular binding configuration.

The analysis of the variance reorganization energy in Eq. (19) in terms of the water and protein components is more non-trivial and requires considering cross-correlations between the protein and water fluctuations. The individual components λ_p^{var} and λ_w^{var} are often found to be significantly larger than the total λ^{var}. The cross-term λ_{pw}^{var} is therefore negative, pointing to a mutual cancellation between the water and protein fluctuations.[11] The physics of this cancellation is easy to understand in terms of domains of water polarized by the charged surface residues and adiabatically following their elastic motions (Fig. 5(a)).[45] The dipoles of waters polarized by a charged residue create surface charges of the opposite sign, thus screening the electrostatic potential of the residue. The overall cancellation of the direct and cross contributions to λ^{var}, however, strongly varies among the proteins studied so far and is probably largely determined by the specific distribution of the surface charge for a given protein.[45] This observation links sequence to function, since the distribution of the surface charge is encoded in the sequence and the fold.

Given the complexity of the mutual cancelation of the water and protein electrostatic fluctuations, one wonders if at least one of the components can be adequately modeled. This attempt was undertaken[28] within the framework of an elasto-electric model of the protein. The model keeps the atomic charge distribution of a standard force field, but coarse-grains the protein motions into an elastic network of rigid amino acids connected by Hookean springs.[101,102] A heterogeneous scheme of assigning the force constant was applied,[103,104] in which stiffer springs were used for back-bone amino-acids and the springs attached to the ionized surface residues were additionally softened by solvation.[28] The assignment of the spring force constants was tested on the dynamics of amino acid separations produced by long MD simulations. Further, assuming non-Markovian Langevin dynamics of the normal modes diagonalizing the network of amino-acid beads, electrostatic frequency-dependent response functions were constructed. Those can be used to test the consistency with $\chi_p''(\omega)$ (protein component of the loss function) reported by MD simulations.

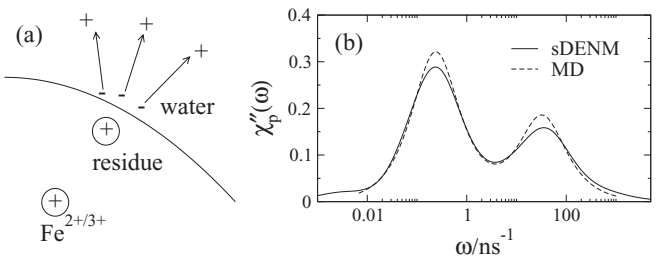

FIG. 5. (a) Cartoon of the water domain polarized by a positively charged surface residue. As in Fig. 1, the redox site is specified by the Fe ion changing its redox state. The preferential orientation of the water dipoles at the surface creates surface charge and an effective electrostatic potential compensating for the potential of the surface residue.[45] The compensation can be incomplete, and the overall effect is determined by the surface charge distribution. (b) The protein component $\chi_p''(\omega)$ of the loss function calculated from MD trajectories of a fully hydrated protein cytochrome B562 (dashed line) and the same property calculated from the solvated dissipative electro-elastic model (sDENM), which coarse-grains the protein to an elastic network of rigid amino acids carrying atomic force-field charges.[28]

These results, from Ref. 28, are shown in Fig. 5(b). The assignment of the slower, nanosecond dynamics of the energy-gap to elastic deformations of the protein is consistent with the electro-elastic coarse-grained model, and the magnitude of λ_p in Eq. (19) can be reproduced. The view that large-amplitude electrostatic noise at the active site is caused by elastic motions altering the protein's charge distribution is supported by both atomistic simulations and formal modeling.

VI. EXPERIMENTAL EVIDENCE

Separate experimental measurements of λ^{St} and λ^{var} reorganization energies can be achieved by optical spectroscopy of transitions changing the charge distribution of a chromophore. The former is one half of the solvent-induced Stokes shift, while the latter is responsible for inhomogeneous broadening of individual vibronic lines in the optical spectrum.[65,105] In cases when the band-shape analysis of optical transitions in proteins is possible, the experimental results point to $\lambda^{var} > \lambda^{St}$, in accord with our suggested picture. The established examples are just a few. A recent example is the absorption and emission spectra of the metal-free cytochrome *c*,[50] which lead to $\chi_G = 2$ (using the Gaussian line-shape fit reported in Ref. 50). A more extensive set of measurements reports band-shapes of fluorescent proteins of various primary colors.[106] Figure 6 shows an example of the band-shape analysis of mStrawberry fluorescent protein,[106] which results in $\chi_G \simeq 1.8$. This latter result is below χ_G obtained in MD simulations of a similar fluorescent protein.[45] The difference might be attributed to a heterogeneous distribution of proteins

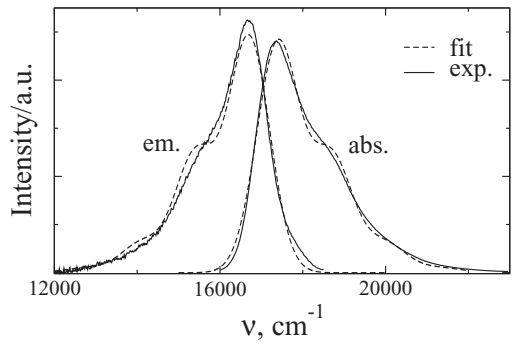

FIG. 6. Absorption and emission lines of mStrawberry fluorescent protein[106] (solid lines) and their fit by vibronic progression of Gaussian lines[65] (dashed lines). The fitting was done with fixed effective frequency of intramolecular vibrations $\nu_v = 1300\ \mathrm{cm}^{-1}$ and the Huang-Rhys factor[65] of $S = 0.5$: $\lambda^{\mathrm{St}} = 344\ \mathrm{cm}^{-1}$, $\lambda^{\mathrm{var}} = 613\ \mathrm{cm}^{-1}$, and $\chi_G = 1.8$.

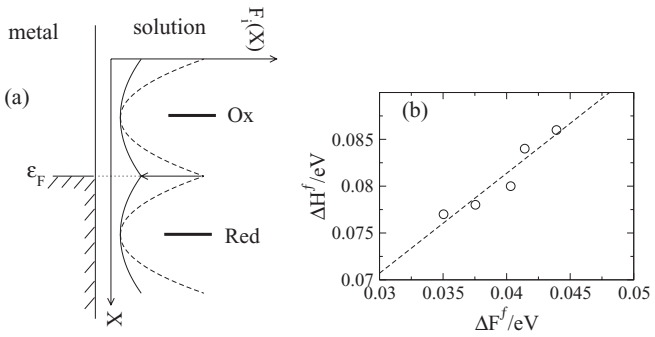

FIG. 7. (a) Cartoon of electrochemical electron transfer. Shown are the metal electrodes with the Fermi energy level ϵ_F and the energy levels of the oxidized (Ox) and reduced (Red) forms in the solution. Zero overpotential leads to symmetric free energy surfaces $F_i(X)$ crossing at the point of resonance of either Ox or Red energy levels with the Fermi energy level of the metal. Introducing the non-Gaussian parameter $\chi_G > 1$ lowers the activation barrier from the Marcus prediction of $\lambda^{\mathrm{St}}/4$ to the value given by Eq. (21) (indicated by the arrow). (b) Experimental $\Delta H^\dagger$ from Ref. 114 vs. $\Delta F^\dagger$ for wild type and a number of mutants of azurin (points). The activation free energy $\Delta F^\dagger$ is calculated from Eq. (21) with λ^{St} from MD simulations[115] and a constant $\chi_G = 7$. The latter choice of χ_G produces a unity slope of the linear regression (shown by the dashed line) and a non-zero intercept, nominally corresponding to the activation entropy. The required value of χ_G is consistent with $\chi_G \simeq 7.8$ reported from MD simulations of a structurally similar protein plastocyanin.[11]

occupying different sub-states along the q-coordinate in Fig. 4 and thus effectively reducing χ_G.

An alternative approach to extract λ^{St} and λ^{var} separately is through electrochemistry. For globally non-Gaussian statistics of the energy gap described here, the activation barrier of electrochemical discharge is given as $\Delta F^\dagger = (\lambda^{\mathrm{St}} + e\eta)^2/(4\lambda^{\mathrm{var}})$, where η is the electrode overpotential and e is the elementary charge. The activation free energy at $\eta = 0$ is then

$$\Delta F^\dagger = \frac{\lambda^r}{4} = \frac{\lambda^{\mathrm{St}}}{4\chi_G}. \tag{21}$$

Cyclic voltammetry of redox proteins immobilized on self-assembled monolayers has consistently produced low activation barriers.[107–114] The values of reorganization energy extracted from these measured barriers according to the standard Marcus recipe ($\chi_G = 1$ in Eq. (21)) fall in the range of 0.1–0.4 eV, often inconsistent with independent estimates. The lowering of the barrier with increasing χ_G is, however, exactly what the current model predicts (depression of the barrier shown by the vertical arrow in Fig. 7(a) and by Eq. (21)).

A good study case to illustrate the origin of discrepancies is electron transfer in a family of azurin mutants for which both experimental activation enthalpies[114] and λ^{St} from extensive MD simulations[115] have been reported. Experimental activation enthalpies $\Delta H^\dagger = \Delta F^\dagger + T\Delta S^\dagger$ for four mutants and wild-type azurin,[114] are plotted in Fig. 7(b) against $\Delta F^\dagger$ calculated from Eq. (21) with λ^{St} from simulations.[115] Getting a near-unity slope between $\Delta H^\dagger$ and $\Delta F^\dagger$ requires $\chi_G \simeq 7$, which is taken as a constant value. This value is consistent with $\chi_G \simeq 7.8$ calculated from MD simulations of plastocyanin,[11] a blue copper protein from the same family and with a similar structure.

The value of χ_G can be extracted from the dependence of the rate on the electrode overpotential,[113] which in the current description is given by the following equation:

$$k(\eta) \propto \mathrm{erfc}\left(\frac{\lambda^{\mathrm{St}} + e\eta}{\sqrt{2}\sigma(T)}\right). \tag{22}$$

Here, erfc(x) is the complementary error function. A combination of temperature and overpotential dependencies might appear, at first glance, as a sensible approach to fit Eq. (22) to experiment. The use of the Arrhenius kinetics might, however, be misleading for protein electron transfer, as we discuss next.

Simulation studies of redox proteins offer specific predictions regarding the temperature dependence of the rate of protein electron transfer.[45,116] The low-temperature portion of the energy-gap variance commonly follows the prediction of the fluctuation-dissipation theorem[64,117] established for a thermal bath of harmonic oscillators, $\sigma(T)^2 \propto T$ (Fig. 8). The rate constant

$$k \propto \exp\left[-\frac{(X_1)^2}{2\sigma(T)^2}\right] \tag{23}$$

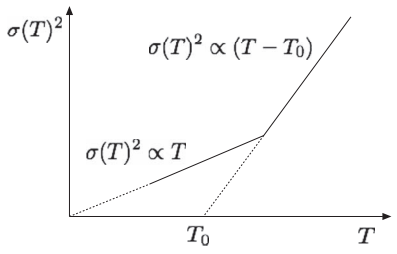

FIG. 8. Cartoon illustrating the typical temperature dependence of the variance of the donor-acceptor energy gap in protein electron transfer. The low-temperature portion follows the rules established for a bath of harmonic oscillators, $\sigma(T)^2 \propto T$, with the resulting Arrhenius law for the rate constant of electron transfer. The high-temperature part of the variance inflects into a stronger temperature variation. When the high-temperature portion of the plot is fitted to a straight line $\sigma(T)^2 \propto (T - T_0)$, electron transfer rate follows the Vogel-Fulcher-Tammann kinetics (Eq. (24)).

then follows the Arrhenius law. On the contrary, the entrance of slow elastic motions of the proteins into the observation window[79] at higher temperatures implies a faster than linear growth of $\sigma(T)^2$ [Fig. (8)].[45,116] In the high-temperature range, the variance can be approximated by a linear function,[45] $\sigma(T)^2 \propto (T - T_0)$. This temperature dependence, substituted into Eq. (23), leads to the Vogel-Fulcher-Tammann kinetics often found for fragile glass-formers,[53]

$$k \propto \exp\left[-\frac{AT_0}{T - T_0}\right]. \tag{24}$$

Equations (23) and (24) make specific predictions regarding the magnitude and the temperature dependence of the electrochemical transfer coefficient $\alpha = \partial(\Delta F^{\dagger}(\eta))/\partial(e\eta)|_{\eta=0}$. One gets

$$\alpha(T) = \frac{1}{2\chi_G}\frac{T}{T - T_0}, \tag{25}$$

where χ_G is calculated at some temperature and left unchanged. $\chi_G > 1$ means $\alpha(T) < 0.5$ in Eq. (25). This result can potentially be masked in measurements done at a fixed temperature by the compensating effect of the temperature term in the second part of Eq. (25). Given that $T_0 \simeq (0.5 - 0.7)T$ for room-temperature measurements, the temperature term in Eq. (25) can produce a factor of 2–3.

VII. EFFICIENCY OF ENERGY CHAINS IN BIOLOGY

Energy in living organisms is supplied by the gradient of proton concentration across the cellular membrane. This energy source is common to all types of cells and is considered to be one of the two founding principles of life,[118] the storage of genetic information in the DNA is the second one.

The creation of the concentration gradient implies moving protons from the cytoplasm to the intracellular solution. This proton translocation is driven by the transport of electrons across the membrane in the opposite direction, from outside to inside the cell. The electron transport is initiated by reducing agents from food supply or from the energy of light in photosynthetic organisms. In both cases, electrons are injected into a chain of electron-transfer cofactors localized inside the membrane.[56]

The requirement to separate the input and output sites, and to translocate protons at intermediate sites, puts in place the need for a long distance of cross-membrane electron transport, involving many intermediate states. This structural constraint is combined with the energetic constraint requiring that the overall free energy released as heat in many intermediate states should not exceed the difference in redox free energies of the input and output states. Given that this free energy gap typically does not significantly exceed ≈1 eV, many steps in the electron transport chain are nearly reversible. For instance, electron transport in mitochondria involves about 22 intermediate cofactors with the overall change of the driving force (negative of the reaction Gibbs energy) not exceeding 1.1 eV.[56]

Long distance of electron transport and a small driving force are conflicting requirements. One needs a positive driving force to direct electrons along the chain of hops between the cofactors to avoid reversibility. On the other hand, a large number of such hops within a small overall free energy gap leaves only a small driving force for a single electron-transfer event. This, in addition to the danger of reversing the electron flow, has to result in a significant slowing down of the entire energy chain. These mechanistic and energetic constraints, mostly dictated by the structural arrangement of the cofactors in the membrane and the amount of the redox energy provided by food, pose the question of how biology achieves its energy production goals and, in case of bacterial photosynthesis, does it with a high quantum yield of generating an across-membrane electron-hole pair per absorbed photon.[119]

The new mechanistic properties of protein electron transfer, first revealed by simulations[43,52] and more recently supported by electro-elastic models of proteins,[28] provide the resolution of the paradox of energetic efficiency of biology. As discussed above, two components are important here, the breadth of electrostatic fluctuations produced by the protein-water interface and the ability to dynamically freeze some of the nuclear degrees of freedom on the time-scale of the reaction.

The requirement to dynamically freeze a part of the spectrum of nuclear modes to prevent the system from full equilibration, and thus gaining a large λ^{St} consistent with $\chi_G \simeq 1$, imposes some significant limitations on the time-scales available to elementary electron-transfer steps in energy-efficient electron transport chains. This is illustrated in Fig. 9. It shows the range of time-scales at which the operation of enzymatic reactions can both take advantage of a broad distribution of electrostatic fluctuations and avoid the penalty of a large λ^{St}.

The rightmost part of the diagram in Fig. 9 indicates reactions occurring on the time-scale of picoseconds. This

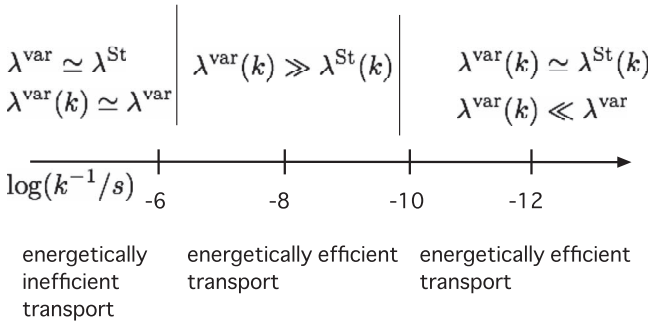

FIG. 9. Time arrow classifying elementary steps of biological electron transfer. The rightmost reaction time window shows ultrafast picosecond reactions activated by ballistic vibrational modes of the medium. All dissipative dynamics of the protein-water interface are dynamically frozen on this time window and the reaction operates according to the classical Marcus prescription of crossing parabolas, but with an effective reorganization energy $\lambda^{var}(k) \ll \lambda^{var}$ and, correspondingly, dynamically arrested solvation component of the reaction free energy.[52,58] The leftmost time window corresponds to slow reactions fully equilibrated to the nuclear modes of the protein-water system. An activationless electronic transition is energetically inefficient in this reaction window since the conformation change resulting from altering the redox state leads to a large energy loss $\Delta F \simeq -\lambda^{St} \simeq -\lambda^{var}$ to heat. The intermediate window allows energetically efficient activationless electron transfer, when the energy lost to heat is $-\lambda^{St}/\chi_G$, $\chi_G > 1$. The vertical lines separating the regions are not intended to represent exact boundaries and specify only approximate, order-of-magnitude reaction times.

is the time-scale of primary charge separation in bacterial photosynthesis.[119] Most of the nuclear modes contributing to the reorganization energy are frozen on the reaction time $\tau_{obs} = k^{-1}$, leading to $\lambda^{var}(k) \simeq 0.36$ eV, instead of $\lambda^{var} \simeq 2.5$ eV calculated from long MD trajectories. Since only fast ballistic modes operate on this time-scale, $\chi_G \simeq 1$ and the reaction rates can be calculated from the standard picture of Marcus crossing parabolas characterized by an effective reorganization energies $\lambda(k)$ and, correspondingly, effective reaction free energies.[52,58]

The leftmost part of the diagram shows slow reactions, slower than the conformational transition of the protein associated with changing redox state. All nuclear modes coupled to the energy-gap reaction coordinate fully explore their phase space and the standard prescriptions of the equilibrium thermodynamics of Gaussian fluctuations apply.[33–35,55] In this time window, an activationless transition loses a significant energy $\Delta F \simeq -\lambda^{St} \simeq -\lambda^{var}$. To avoid such energy losses, reactions on this time-scale proceed with nearly zero driving force.[56] Since this route leads to a significant slowing down, such reactions are often accompanied by proton transfer,[120] shifting ΔF in the favorable direction.

Finally, reactions on the nanosecond time-scale (middle time window) proceed with partial dynamical freezing of the conformational degrees of freedoms, resulting in $\chi_G > 1$. According to Eq. (8) the energy λ^r released to heat in an activationless transition is scaled down by a factor of χ_G. The shallow, but not widely separated free energy surfaces relevant to this time window allow multiple electron transfer events within a narrow range of the reaction driving force.

VIII. CONCLUDING REMARKS

The idea of fine tuning, ascribed to evolution, of either redox potentials or reorganization energies of cofactors involved in functionally significant biological interactions is often discussed in the literature. Fine tuning clearly collides with the requirement of robust operation, little sensitive to external conditions and occasional mutations.[121] The view of biological electron transfer offered here is in a way opposite to the concept of fine tuning. Both simulations and formal modeling suggest that biological redox machines operate in a highly fluctuating nano-scale environment,[122,123] characterized, in particular, by a high level of electrostatic noise. They take advantage of this noise by allowing shallow landscapes of electron transfer free energies achieved by adjusting rates of electronic transitions and residence times on the redox cofactors to the time-windows at which electrostatic fluctuations of the interface are explored, but conformational transitions, coupled to changes in the redox state and occurring on longer time-scales, are not. Efficient electron transport thus occurs through a sequence of conformationally quenched cofactors, dynamically restricted from altering their equilibrium conformations, but sensitive to faster elastic fluctuations of the protein-water interface. This requirement cannot be accommodated for all steps in the chain and slower electron-transfer steps have to operate at nearly zero driving force, with the resulting, and real, danger of reversibility.[124]

ACKNOWLEDGMENTS

This research was supported by the National Science Foundation (NSF) (CHE-1213288). The author is grateful to Mikhail Drobizhev for sharing spectra of fluorescent proteins.

[1] R. A. Marcus, Annu. Rev. Phys. Chem. **15**, 155 (1964).
[2] R. A. Marcus and N. Sutin, Biochim. Biophys. Acta **811**, 265 (1985).
[3] The residence time of waters in hydration shells of $Fe^{2+/3+}$ ions ranges between 10^{-7} s (Fe^{2+}) and 10^{-3} s (Fe^{3+}), see G. W. Neilson and J. E. Enderby, Adv. Inorg. Chem. **34**, 195 (1989).
[4] F. O. Raineri and H. L. Friedman, Adv. Chem. Phys. **107**, 81 (1999).
[5] M. D. Newton, Adv. Chem. Phys. **106**, 303 (1999).
[6] L. L. Conte, C. Chothia, and J. Janin, J. Mol. Biol. **285**, 2177 (1999).
[7] D. J. Barlow and J. M. Thornton, Biopolymers **25**, 1717 (1986).
[8] Y. Levy and J. Onuchic, Annu. Rev. Biophys. Biomol. Struct. **35**, 389 (2006).
[9] N. Giovambattista, C. F. Lopez, P. J. Rossky, and P. G. Debenedetti, Proc. Natl. Acad. Sci. U.S.A. **105**, 2274 (2008).
[10] F. Pizzitutti, M. Marchi, F. Sterpone, and P. J. Rossky, J. Phys. Chem. B **111**, 7584 (2007).
[11] D. N. LeBard and D. V. Matyushov, J. Phys. Chem. B **114**, 9246 (2010).
[12] C. Y. Lee, J. A. McCammon, and P. J. Rossky, J. Chem. Phys. **80**, 4448 (1984).
[13] C. L. McFearin, D. K. Beaman, F. G. Moore, and G. L. Richmond, J. Phys. Chem. C **113**, 1171 (2009).
[14] S. Nihonyanagi, S. Yamaguchi, and T. Tahara, J. Chem. Phys. **130**, 204704 (2009).
[15] D. Verreault, W. Hua, and H. C. Allen, J. Phys. Chem. Lett. **3**, 3012 (2012).
[16] J. A. Mondal, S. Nihonyanagi, S. Yamaguchi, and T. Tahara, J. Am. Chem. Soc. **134**, 7842 (2012).
[17] M. Gerstein and C. Chothia, Proc. Natl. Acad. Sci. U.S.A. **93**, 10167 (1996).
[18] D. I. Svergun, S. Richard, M. H. J. Koch, Z. Sayers, S. Kuprin, and G. Zaccai, Proc. Natl. Acad. Sci. U.S.A. **95**, 2267 (1998).
[19] D. Russo, J. Teixeira, L. Kneller, J. R. D. Copley, J. Ollivier, S. Perticaroli, E. Pellegrini, and M. A. Gonzalez, J. Am. Chem. Soc. **133**, 4882 (2011).
[20] M. Heyden, D. J. Tobias, and D. V. Matyushov, J. Chem. Phys. **137**, 235103 (2012).
[21] L. Comez, L. Lupi, A. Morresi, M. Paolantoni, P. Sassi, and D. Fioretto, J. Phys. Chem. Lett. **4**, 1188 (2013).
[22] K. A. Henzler-Wildman, V. Thai, M. Lei, M. Ott, M. Wolf-Watz, T. Fenn, E. Pozharski, M. A. Wilson, G. A. Petsko, M. Karplus, C. G. Hubner, and D. Kern, Nature (London) **450**, 838 (2007).
[23] A. J. Wand, Nat. Struct. Biol. **8**, 926 (2001).
[24] H. Frauenfelder, G. Chen, J. Berendzen, P. W. Fenimore, H. Jansson, B. H. McMahon, I. R. Stroe, J. Swenson, and R. D. Young, Proc. Natl. Acad. Sci. U.S.A. **106**, 5129 (2009).
[25] M. C. Thielges and M. D. Fayer, Acc. Chem. Res. **45**, 1866 (2012).
[26] P. I. Zhuravlev and G. A. Papoian, Q. Rev. Biophys. **43**, 295 (2010).
[27] Z. Wang, C. E. Bertrand, W.-S. Chiang, E. Fratini, P. Baglioni, A. Alatas, E. E. Alp, and S.-H. Chen, J. Phys. Chem. B **117**, 1186 (2013).
[28] D. R. Martin and D. V. Matyushov, J. Chem. Phys. **137**, 165101 (2012).
[29] S. Sen, D. Andreatta, S. Y. Ponomarev, D. L. Beveridge, and M. A. Berg, J. Am. Chem. Soc. **131**, 1724 (2009).
[30] D. V. Matyushov, J. Phys. Chem. B **115**, 10715 (2011).
[31] M. Lax, J. Chem. Phys. **20**, 1752 (1952).
[32] L. D. Zusman, Chem. Phys. **49**, 295 (1980).
[33] J. K. Hwang and A. Warshel, J. Am. Chem. Soc. **109**, 715 (1987).
[34] R. A. Kuharski, J. S. Bader, D. Chandler, M. Sprik, M. L. Klein, and R. W. Impey, J. Chem. Phys. **89**, 3248 (1988).
[35] M. Tachiya, J. Phys. Chem. **93**, 7050 (1989).
[36] G. King and A. Warshel, J. Chem. Phys. **93**, 8682 (1990).
[37] A. Warshel and W. W. Parson, Annu. Rev. Phys. Chem. **42**, 279 (1991).
[38] S. K. Pal and A. H. Zewail, Chem. Rev. **104**, 2099 (2004).
[39] L. Zhang, L. Wang, Y.-T. Kao, W. Qiu, Y. Yang, O. Okobiah, and D. Zhong, Proc. Natl. Acad. Sci. U.S.A. **104**, 18461 (2007).

[40]P. Abbyad, X. Shi, W. Childs, T. B. McAnaney, B. E. Cohen, and S. G. Boxer, J. Phys. Chem. B **111**, 8269 (2007).
[41]D. Zhong, S. K. Pal, and A. H. Zewail, Chem. Phys. Lett. **503**, 1 (2011).
[42]B. Bagchi, Chem. Phys. Lett. **529**, 1 (2012).
[43]D. N. LeBard and D. V. Matyushov, J. Phys. Chem. B **112**, 5218 (2008).
[44]A. A. Golosov and M. Karplus, J. Phys. Chem. B **111**, 1482 (2007).
[45]D. R. Martin and D. V. Matyushov, J. Phys. Chem. B **116**, 10294 (2012).
[46]X. J. Jordanides, M. J. Lang, X. Song, and G. R. Fleming, J. Phys. Chem. B **103**, 7995 (1999).
[47]D. Toptygin, A. M. Gronenborn, and L. Brand, J. Phys. Chem. B **110**, 26292 (2006).
[48]K. Sahu, S. K. Mondal, S. Ghosh, D. Roy, and K. Bhattacharyya, J. Chem. Phys. **124**, 124909 (2006).
[49]K. Bhattacharyya, Chem. Commun. **2008**, 2848.
[50]J. Tripathy and W. F. Beck, J. Phys. Chem. B **114**, 15958 (2010).
[51]D. V. Matyushov, J. Chem. Phys. **130**, 164522 (2009).
[52]D. N. LeBard and D. V. Matyushov, Phys. Chem. Chem. Phys. **12**, 15335 (2010).
[53]C. A. Angell, Science **267**, 1924 (1995).
[54]P. K. Ghorai and D. V. Matyushov, J. Phys. Chem. B **110**, 1866 (2006).
[55]D. W. Small, D. V. Matyushov, and G. A. Voth, J. Am. Chem. Soc. **125**, 7470 (2003).
[56]D. G. Nicholls and S. J. Ferguson, *Bioenergetics 3* (Academic Press, London, 2002).
[57]R. A. Marcus, J. Chem. Phys. **43**, 1261 (1965).
[58]D. N. LeBard, V. Kapko, and D. V. Matyushov, J. Phys. Chem. B **112**, 10322 (2008).
[59]R. A. Marcus, Rev. Mod. Phys. **65**, 599 (1993).
[60]C. H. Bennett, J. Comput. Phys. **22**, 245 (1976).
[61]L. Reynolds, J. A. Gardecki, S. J. V. Frankland, and M. Maroncelli, J. Phys. Chem. **100**, 10337 (1996).
[62]S. Mukamel, *Principles of Nonlinear Optical Spectroscopy* (Oxford University Press, New York, 1995).
[63]G. R. Fleming and M. Cho, Annu. Rev. Phys. Chem. **47**, 109 (1996).
[64]J. P. Hansen and I. R. McDonald, *Theory of Simple Liquids* (Academic Press, Amsterdam, 2003).
[65]M. Bixon and J. Jortner, Adv. Chem. Phys. **106**, 35 (1999).
[66]R. Jimenez, G. R. Fleming, P. V. Kumar, and M. Maroncelli, Nature (London) **369**, 471 (1994).
[67]N. Gayathri and B. Bagchi, J. Phys. Chem. **100**, 3056 (1996).
[68]C. Creutz, M. D. Newton, and N. Sutin, J. Photochem. Photobiol., A **82**, 47 (1994).
[69]M. Cascella, A. Magistrato, I. Tavernelli, P. Carloni, and U. Rothlisberger, Proc. Natl. Acad. Sci. U.S.A. **103**, 19641 (2006).
[70]X. Xie, S. I. Gorelsky, R. Sarangi, D. K. Garner, H. J. Hwang, K. O. Hodgson, B. Hedman, Y. Lu, and E. I. Solomon, J. Am. Chem. Soc. **130**, 5194 (2008).
[71]E. E. Hammi, C. Houee-Levin, J. Rezac, B. Levy, I. Demachy, L. Baciou, and A. de la Lande, Phys. Chem. Chem. Phys. **14**, 13872 (2012).
[72]M. G. I. Galinato, J. G. Kleingardner, S. E. J. Bowman, E. E. Alp, J. Zhao, K. L. Bren, and N. Lehnert, Proc. Natl. Acad. Sci. U.S.A. **109**, 8896 (2012).
[73]*Cytochrome C: A Multidisciplinary Approach*, edited by R. A. Scott and A. G. Mauk (University Science Books, Sausalito, CA, 1996).
[74]A. N. Volkov, S. Vanwetswinkel, K. Water, and N. A. J. Nuland, J. Biomol. NMR **52**, 245 (2012).
[75]K. Henzler-Wildman and D. Kern, Nature (London) **450**, 964 (2007).
[76]D. V. Matyushov, Acc. Chem. Res. **40**, 294 (2007).
[77]U. Mandal, S. Ghosh, S. Dey, A. Adhikari, and K. Bhattacharyya, J. Chem. Phys. **128**, 164505 (2008).
[78]D. V. Matyushov, J. Phys. Chem. Lett. **3**, 1644 (2012).
[79]D. V. Matyushov and A. Y. Morozov, Phys. Rev. E **84**, 011908 (2011).
[80]D. Laage, G. Stirnemann, F. Sterpone, R. Rey, and J. T. Hynes, Annu. Rev. Phys. Chem. **62**, 395 (2011).
[81]T. Li, A. A. Hassanali, and S. J. Singer, J. Phys. Chem. B **112**, 16121 (2008).
[82]P. F. Barbara, T. J. Meyer, and M. A. Ratner, J. Phys. Chem. **100**, 13148 (1996).
[83]D. Andreatta, J. L. Pérez, S. A. Kovalenko, N. P. Ernsting, C. J. Murphy, R. S. Coleman, and M. A. Berg, J. Am. Chem. Soc. **127**, 7270 (2005).
[84]N. Ito, K. Duvvuri, D. V. Matyushov, and R. Richert, J. Chem. Phys. **125**, 024504 (2006).
[85]G. van der Zwan and J. T. Hynes, J. Chem. Phys **78**, 4174 (1983).
[86]H. Sumi and R. A. Marcus, J. Chem. Phys **84**, 4894 (1986).
[87]G. C. Walker, E. Åkesson, A. E. Johnson, N. E. Levinger, and P. F. Barbara, J. Phys. Chem. **96**, 3728 (1992).
[88]H. Pal, H. Shirota, K. Tominaga, and K. Yoshihara, J. Chem. Phys. **110**, 11454 (1999).
[89]D. Thirumalai, E. P. O'Brien, G. Morrison, and C. Hyeon, Annu. Rev. Biophys. **39**, 159 (2010).
[90]R. G. Palmer, Adv. Phys. **31**, 669 (1982).
[91]P. W. Fenimore, H. Frauenfelder, B. H. McMahon, and R. D. Young, Proc. Natl. Acad. Sci. U.S.A. **101**, 14408 (2004).
[92]D. V. Matyushov, Chem. Phys. **351**, 46 (2008).
[93]A. D. Friesen and D. V. Matyushov (unpublished).
[94]G. Loffler, H. Schreiber, and O. Steinhauser, J. Mol. Biol. **270**, 520 (1997).
[95]L. Nilsson and B. Halle, Proc. Natl. Acad. Sci. U.S.A. **102**, 13867 (2005).
[96]T. Rudas, C. Schröder, S. Boresch, and O. Steinhauser, J. Chem. Phys. **124**, 234908 (2006).
[97]D. V. Matyushov, J. Chem. Phys. **136**, 085102 (2012).
[98]D. N. LeBard and D. V. Matyushov, J. Phys. Chem. B **113**, 12424 (2009).
[99]F. Meschi, F. Wiertz, L. Klauss, A. Blok, B. Ludwig, A. Merli, H. A. Heering, G. L. Rossi, and M. Ubbink, J. Am. Chem. Soc. **133**, 16861 (2011).
[100]Q. Bashir, S. Scanu, and M. Ubbink, FEBS J. **278**, 1391 (2011).
[101]M. M. Tirion, Phys. Rev. Lett. **77**, 1905 (1996).
[102]A. R. Atilgan, S. R. Durell, R. L. Jernigan, M. C. Demirel, O. Keskin, and I. Bahar, Biophys. J. **80**, 505 (2001).
[103]D. Ming and M. E. Wall, Phys. Rev. Lett. **95**, 198103 (2005).
[104]K. Moritsugu and J. C. Smith, Biophys. J. **93**, 3460 (2007).
[105]D. V. Matyushov and M. D. Newton, J. Phys. Chem. A **105**, 8516 (2001).
[106]M. Drobizhev, N. S. Makarov, S. E. Tillo, T. E. Hughes, and A. Rebane, J. Phys. Chem. B **116**, 1736 (2012).
[107]J. Hirst and F. A. Armstrong, Anal. Chem. **70**, 5062 (1998).
[108]Q. Chi, J. Zhang, J. E. T. Andersen, and J. Ulstrup, J. Phys. Chem. B **105**, 4669 (2001).
[109]L. J. C. Jeuken, J. P. McEvoy, and F. A. Armstrong, J. Phys. Chem. B **106**, 2304 (2002).
[110]P. Hildebrandt and D. H. Murgida, Bioelectrochemistry **55**, 139 (2002).
[111]Y. Guo, J. Zhao, X. Yin, X. Gao, and Y. Tian, J. Phys. Chem. C **112**, 6013 (2008).
[112]D. E. Khoshtariya, T. D. Dolidze, M. Shushanyan, K. L. Davis, D. H. Waldeck, and R. van Eldik, Proc. Natl. Acad. Sci. U.S.A. **107**, 2757 (2010).
[113]H. Khoa Ly, N. Wisitruangsakul, M. Sezer, J.-J. Feng, A. Kranich, I. M. Weidinger, I. Zebger, D. H. Murgida, and P. Hildebrandt, J. Electroanal. Chem. **660**, 367 (2011).
[114]S. Monari, G. Battistuzzi, C. A. Bortolotti, S. Yanagisawa, K. Sato, C. Li, I. Salard, D. Kostrz, M. Borsari, A. Ranieri, C. Dennison, and M. Sola, J. Am. Chem. Soc. **134**, 11848 (2012).
[115]L. Paltrinieri, M. Borsari, A. Ranieri, G. Battistuzzi, S. Corni, and C. A. Bortolotti, J. Phys. Chem. Lett. **4**, 710 (2013).
[116]D. N. LeBard and D. V. Matyushov, Phys. Rev. E **78**, 061901 (2008).
[117]D. A. McQuarrie, *Statistical Mechanics* (University Science Books, Sausalito, CA, 2000).
[118]N. Lane, *Power, Sex, Suicide. Mitochondria and the Meaning of Life* (Oxford University Press, Oxford, 2005).
[119]A. J. Hoff and J. Deisenhofer, Phys. Rep. **287**, 1 (1997).
[120]A. R. Crofts, Biochim. Biophys. Acta **1655**, 77 (2004).
[121]D. Noy, C. C. Moser, and P. L. Dutton, Biochim. Biophys. Acta **1757**, 90 (2006).
[122]R. D. Astumian, Annu. Rev. Biophys. **40**, 289 (2011).
[123]P. C. Whitford, K. Y. Sanbonmatsu, and J. N. Onuchic, Rep. Prog. Phys. **75**, 076601 (2012).
[124]A. Osyczka, C. C. Moser, and P. L. Dutton, Trends Biochem. Sci. **30**, 176 (2005).